Mass Transfer Coefficients of Carbon Dioxide in Aqueous Blends of Monoethanolamine and Glycerol Using Wetted-Wall Column

Shervan Babamohammadi [a], Rozita Yusoff [a], Mohamed Kheireddine Aroua [b,c,*], Tohid N.Borharni [d,*]

[a] Department of Chemical Engineering Department, Faculty of Engineering, University of Malaya, 50603 Kuala Lumpur, Malaysia

[b] Research Centre for Carbon Dioxide Capture and Utilisation (CCDCU), School of Engineering and Technology, Sunway University, Bandar Sunway, 47500, Petaling Jaya, Malaysia

[c] Department of Engineering, Lancaster University, Lancaster LA1 4YW, UK

[d] School of Engineering, Division of Chemical Engineering, University of Wolverhampton, Wolverhampton, WV1 1LY, United Kingdom

Abstract

There is an urgent need for CO_2 capture development because of the global warming crisis. Recently CO_2 absorption by the mixture of Monoethanolamine (MEA) and glycerol, as an eco-friendly solvent, has been considered due to its promising performance and low technical and environmental impacts. However, more aspects of this process, especially mass transfer coefficients, need to be studied further. In this work, a bench-scale wetted-wall column was used to find the CO_2 mass transfer coefficients in the aqueous blends of MEA (25 wt%) and glycerol (5-20 wt%). The experiments were performed nearly to the industrial conditions of flue gas at atmospheric pressure and three different temperatures (313, 323, and 333 K). The gas flow rate was maintained around 0.17±0.01 stdL/s, and the CO_2 partial pressure was in the range of 1-15 kPa. The findings revealed that increasing the glycerol to 10 wt% improves the overall mass transfer (K_G), and adding more glycerol up to 20 wt% decreases the K_G. The gas-side mass transfer resistance ($1/k_g$) found to be negligible. Thus, the primary mass transfer resistance was in the liquid phase. It is also found that the solution with 10 wt% glycerol and

* Corresponding authors. Email addresses: kheireddinea@sunway.edu.my (Prof Mohamed Kheireddine Aroua), t.borhani@wlv.ac.uk (Dr Tohid Borhani)

25 wt% MEA (10G25M) had the highest liquid-side mass transfer coefficient (k_g') among the other solutions. The 10G25M showed a comparable and even better absorption rate than solutions with a higher concentration of MEA studied in the literature. Compared with industrial-grade, the k_g' of the 10G25M was over two times higher than the 30 wt% MEA solution.

Keywords:

Mass Transfer Coefficient, Glycerol, Carbon Dioxide, Monoethanolamine, Absorption, Wetted-Wall Column

Nomenclatures

Symbols	
A	Contact area, cm^2
d_h	Hydraulic diameter of the wetted wall column, cm
D_{CO_2}	Diffusion coefficient of CO_2 in the gas phase, cm^2/s
g_c	Gravitational constant, m/s^2
G	Gas volumetric flow rate, ml/s
h	Height of the column, cm
K_G	Overall Mass Transfer Coefficient, $mol/cm^2.Pa.s$
k_g	Gas-side mass transfer coefficient, $mol/cm^2.Pa.s$
k_l	Liquid-side mass transfer coefficient, $mol/cm^2.Pa.s$
k_g'	Total Liquid-side mass transfer coefficient with chemical reaction, $mol/cm^2.Pa.s$
k_l^0	Liquid-side physical mass transfer coefficient, cm/s
M_{CO_2}	CO_2 molecular weight, g/mol
P_{total}	The total pressure, atm
$P_{CO_2}^*$	CO_2 partial pressure in the system, Pa
P_{CO_2}	CO_2 partial pressure in the inlet gas, Pa
Q_{sol}	Liquid flow rate, ml/s
R_p	Pump rotary power, rpm
u_s	Superficial velocity, cm/s
V_m	Molar volume of an ideal gas, ml/mol
W	Wetted perimeter, cm
Greek Symbols	
α_{CO_2}	CO_2 loading, mol CO_2/mol amine
Θ	Dimensionless driving force
ΔC	Cyclic capacity, mol CO_2/total mass
ρ_{sol}	Solution density, g/cm^3
ρ_w	water density, g/cm^3
δ	Liquid film thickness, cm
τ	Gas-liquid contact time, s
μ	Viscosity, mPa.s
η	Dimensionless penetration distance
Dimensionless groups	
Sh	Sherwood number
Re	Reynolds number
Sc	Schmidt number
Abbreviations	
DESs	Deep Eutectic Solvents
DPT	Differential Pressure Transmitter
ILs	Ionic Liquids
MDEA	Methyl diethanolamine
MEA	Monoethanolamine
2MPZ	2methylpiperazine
NMP	N-methyl-2-pyrolidone
PZ	Piperazine
WWC	Wetted-wall column

1 Introduction

Global warming, caused by greenhouse gases such as CO_2, is one of the world's current critical problems [1]. Chemical and physical absorption are techniques for removing CO_2 from other gases in the exhaust gases of the power plants [2]. Between different solvents that have been used for the absorption of CO_2, alkanolamine solutions have the highest applications. However, there are some significant drawbacks in using various amines, such as a high rate of energy consumption during regeneration, a high rate of equipment corrosion, and the need for a sufficient absorber volume. As a result, developing a new cost-effective and environmentally friendly solution is essential. [3].

In recent years, researchers have been searching for more cost-effective, non-toxic, productive, and reliable CO_2 removal solvents [4, 5]. Moioli, et al. [6] compared potassium-taurate to the conventional MEA solvent as a possible solvent for post-combustion CO_2 capture. They discovered that using potassium-taurate rather than conventional MEA would increase the overall CO_2 absorption efficiency. Their findings from the techno-economic analysis suggest that both processes' capital and operational costs are comparable, but the conventional MEA process is more costly. In the other studies, the ionic liquids (ILs) have been proposed as a potential solvent for CO_2 removal due to their special properties, such as wide liquid range, low vapour pressure, tuneable physicochemical composition, chemical and thermal stability, and high CO_2 absorption. However, several ILs are barely biodegradable, hazardous, and costly to absorb CO_2 [7]. Deep Eutectic Solvents (DESs) have much of the same physicochemical properties as ILs, though they are biodegradable, non-toxic, and cheap, unlike ILs. [8]. As a result, DESs are used as a more environmentally friendly substitute for traditional organic solvents. Siani, et al. [9] recently tested the solubility of CO_2 in a deep eutectic solvent (phenylacetic acid/TMG DES) at various pressures in the range of 0.1-4 MPa and temperatures ranging from 298 to 333 K. According to their findings, after three absorption-desorption

cycles, each gram of the DES can remove up to 45.5 mg of the CO_2. In another study, a group of researchers at the University of Melbourne has studied the role of antisolvent on aqueous amine solutions [10]. They have developed a new biphasic solvent for CO_2 absorption by blending potassium glycinate (GlyK, reactive species), water (H_2O, solvent) and dimethylformamide (DMF, antisolvent). Their solvent was split into two phases upon CO_2 absorption. The upper aqueous-based phase was free of CO_2 and can be easily separated and recycled to the absorption column and save energy. They found that the solvent with DMF:H_2O volume ratio of 60:40 exhibited 26.1% enhancement in CO_2 absorption capacity (0.433–0.546 mol CO_2/mol GlyK), 38.5% decrease in regeneration time (130–80 min) and 59.1% reduction in relative heat duty compared to the conventional aqueous GlyK solvent. Another research by the same group has utilised a novel rate promoter for aqueous solutions of tertiary amines [11]. They used nano-porous carbonaceous promoters (NCPs) as the promoter and added aqueous N, N-diethylethanolamine (DEEA) as the absorbent. Their solution could enhance the rate of CO_2 absorption at 40 °C by 38.6% and improved the equilibrium CO_2 absorption capacity by 13.2% compared to the typical aqueous DEEA solution.

Among the research to find a new solvent for CO_2 capture, glycerol has recently been developed as an alternative CO_2 absorption solvent. It is more convenient and cheaper than ILs and DES while having promising properties [12, 13]. With regard to environmental efforts, the biodiesel industry has made significant progress, and by-products, such as glycerol generated during biodiesel production [14]. Glycerol ($C_3H_8O_3$) is an alcohol with three carbon chains, each of which contains hydroxyl groups. Glycerol is used in a variety of industries, including medicine, food, and cosmetics [15]. Glycerol's high viscosity and boiling point, as well as its solubility characteristics, are due to the effects of three hydroxyl groups with strong intermolecular hydrogen bonding. Glycerol, for example, is a good solvent for bromine and iodine. It can also be dissolved in alcohols and water but not in hydrocarbons. [16]. Glycerol

is generated primarily by biodiesel and oleochemical plants. Glycerol can be generated as a by-product of a transesterification reaction in the biodiesel production, but it is in a crude form that requires further purification. Approximately 10% of biodiesel production is crude glycerol with 50-55% purity [15, 17]. The liquid glycerol is colourless, hygroscopic, clear, viscous, odourless, and sweet-tasting. At room environment condition, its density is 1.261 g/cm^3, molecular weight is 92.09 g/mol, and viscosity is 1.5 Pa.s. It is non-toxic for humans and environmentally friendly. The boiling point, melting point, and flashpoint of glycerol are 290 ℃, 18 ℃ and 177 ℃, respectively [16, 18]. The biodiesel industry is currently the main source of glycerol supply. Because this industry is rapidly expanding, a large amount of raw glycerol is produced; thus, its market price is steadily declining [19]. According to Tan, et al. [15], the worldwide price of pure glycerol is about 40-50 cents per pound and 3.5-10 cents per pound for crude glycerol.

Advantages of glycerol solutions over conventional solvents render these solutions as an appealing choice for CO_2 absorption systems. While several scientific studies on CO_2 absorption in the mixture of glycerol and aqueous MEA have given impressive outcomes [12, 20, 21], many aspects of this system, such as the absorption rate and mass transfer properties, remain unknown. A thorough understanding of these aspects is essential for developing any new industrial absorption unit incorporating MEA-glycerol technology.

Researchers compared glycerol to ILs in terms of CO_2 removal and found that glycerol, in contrast to ILs, is safe and stable while cheaper and can dissolve CO_2 significantly. These characteristics of glycerol have made it an appealing option to conventional solvents like ammonia, carbonate solution, amines and ILs [12].

The main goal of this research is to conduct a comprehensive experimental investigation of CO_2 mass transfer in an aqueous MEA solution mixed with glycerol by using a Wetted Wall Column setup (WWC). Many researchers have used WWC to measure the absorption rate or

mass transfer coefficients. Rashidi and Mamivand [22] used a WWC to study the mass transfer and absorption rate of CO_2 into Al_2O_3/water nanofluid. Using WWC, they could find that the CO_2 mass transfer was enhanced using Al_2O_3/water nanofluid as the solvent. Similarly, Valeh-e-Sheyda and Afshari [23] measured mass transfer and modelled the CO_2 absorption into a water-based nanofluid system using WWC. In another study, the absorption rate and heat of reaction were measured in a modified WWC by Kim, et al. [24]. They used two aqueous solutions of 30 wt% aqueous MEA and 30 wt% aqueous piperazine as solvents to validate the performance of their new WWC with a typical WWC. Wang, et al. [25] proposed a new phase-change absorbent, a mixture of diethylenetriamine (DETA) and diethylaminoethanol (DEEA), for CO_2 absorption and investigated its mass transfer properties in a WWC. They studied the effect of CO_2 loading, temperature and gas flow rate on the mass transfer coefficient. Song and Rochelle [26] also used a WWC to investigate the reaction kinetics of CO_2 and NaOH in an aqueous glycerol solution. They also found that adding glycerol could increase the absorption rate by 30%, although they mentioned that further adding glycerol could rapidly decrease the absorption rate. In another study by Tunnat, et al. [27], the desorption fluxes of CO_2 from loaded aqueous amine solutions and pure water have been measured with a WWC. Overall, much research has been done on CO_2 absorption using WWC as an experimental setup [28-31]. The results of this study are compared to other related research which used a similar method and presented at the end of the result and discussion section.

This paper presents the experimental investigation of CO_2 absorption rate and mass transfer coefficients in an aqueous MEA and glycerol solution. MEA was used as a base solvent because it is well-studied and widely used in CO_2 absorption systems. Furthermore, it is shown that glycerol's benefits as a physical solvent will mitigate MEA's CO_2 absorption disadvantages.

2 Experimental

2.1 Materials

The CO_2 was provided in the gas cylinder, mixed 15 vol% CO_2 and 85 vol% N_2, from Gaslink Sdn Bhd, Malaysia. The pure N_2 gas cylinder was provided from Linde-Gas, Malaysia. Solvent ingredients (MEA and glycerol) were supplied from MERCK KGaA, Germany, with the purities of 99 wt%. During the experiment, the gas flow rate was controlled by a mass flow controller purchased from Brooks Instruments, USA (Model 5850E four-channel power supply). The CO_2 concentration (vol%) was monitored using a CO_2 analyser from Quantek Instruments, USA (Model 902P). The data from the gas analyser were recorded into the PC using HOBOware software connected to a data logger; both purchased from Onset, USA (Model UX120-006M - HOBO Analog Data Logger). A water bath circulator supplied from Lab Companion JEIO TECH, Korea (Model RW-0525G), was used to control the gas and liquid temperature.

2.2 Apparatus and Experimental Procedure

The MEA 25 wt% was combined with 5 wt%, 10 wt%, and 20 wt% glycerol and diluted with distilled water to make three sets of 1-litre solutions. These solutions are named 5G25M, 10G25M, and 20G25M, respectively. For each experimental run, each solution was carefully blended using a magnetic stirrer for about 30 minutes. The experimental setup was used in another study in the same lab [32]. The wetted-wall column (WWC) was similar to a setup that was constructed by Mshewa [33] and developed by Pacheco [34]. Several studies have been used the same design of column for gas-liquid absorption [26, 30, 31]. The WWC schematic diagram is depicted in **Fig. 1**. A peristaltic pump (Model BT 300-2 from LongerPump) sent the solution from a 5-litre tank to the WWC at a steady rotary speed of 50 rpm. **Eq. (1)** shows the derived correlation between the volumetric flow rate (Q_{sol}), the solution density (ρ_{sol}) and the water density (ρ_w) and pump rotary speed (R_p). In each run, the total volume of solution was

held at 1000 ml. The mass flow controller maintained and regulated the input gas flow. A Differential Pressure Transmitter (DPT) read the difference of pressure between inlet and outlet of the WWC. The gas flow rate was held at around 0.17±0.01 stdL/s and the whole system was at atmospheric pressure. Then in the reactor, the liquid and gas contacted counter-currently similar to the packed column. Each test took about 18-24 hours to reach saturation, depended on the solution and its CO_2 absorption rate and capacity.

$$Q_{sol}\left(\frac{ml}{s}\right) = 0.5108 \times R_p(\text{rpm}) - 0.5192 \times \sqrt{\frac{\rho_{sol}}{\rho_w}} \quad (1)$$

The gas and liquid temperature were regulated by the water bath. Since the gas is dry, it might absorb water and decrease the interfacial temperature. Therefore, before feeding the gas into the reactor, it was passed through the water saturator to avoid any water transferring from the solution to the gas stream and keep the temperature constant. The outlet gas from the reactor consists of moisture which causes the CO_2 analyser to fail; thus, before the gas is injected into the analyser, a drying setup including an ice-bath flask absorbed moisture from the gas for a reliable reading. The CO_2 analyser had a precision of 0.01 vol% and performed in the range of (0.00-25.00) vol%. The data is collected and stored by the data logger linked to the HOBOware programme. All data were collected with 30 seconds intervals and plotted against time. After that, the tabulated information was exported to Microsoft Excel for further analysis.

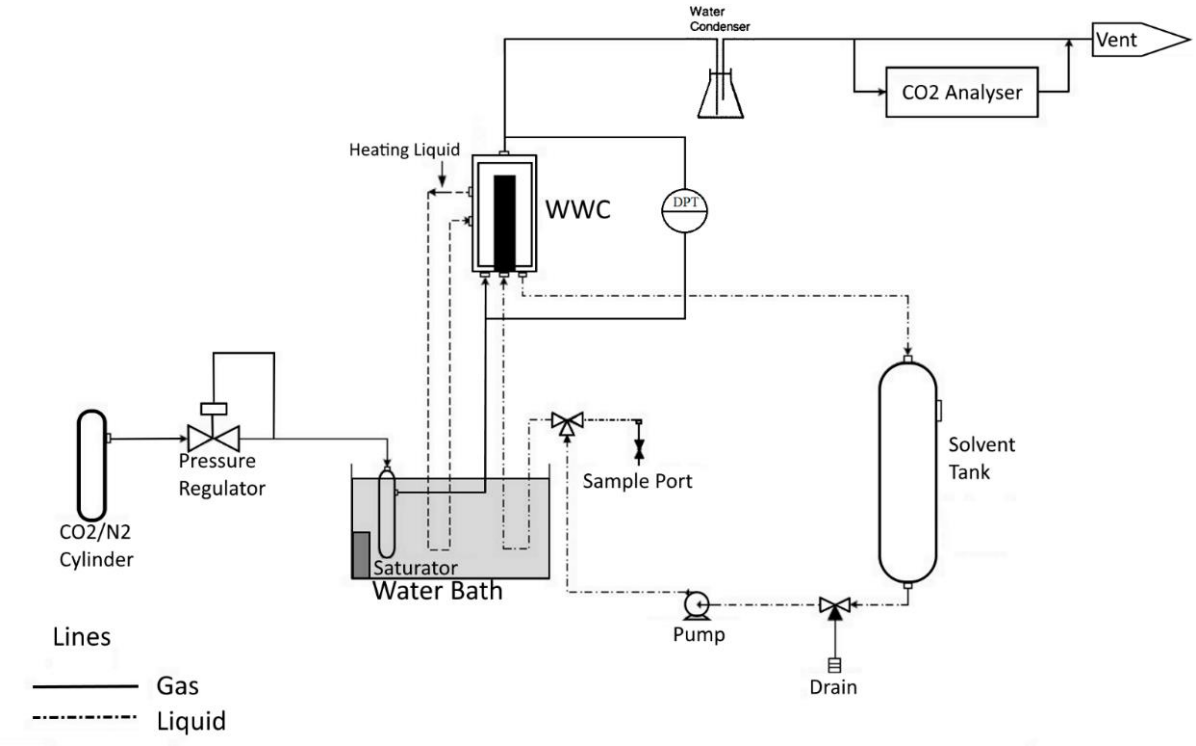

Fig. 1: Process flow diagram of CO_2 absorption with WWC setup.

A mass balance for the CO_2 gas stream around the reactor, assuming the ideal gas law (which is acceptable at low pressure), gives the amount of absorbed CO_2. **Eq. (2)** shows the numerical calculation for the CO_2 mass balance, where t_is are reading intervals from t_0 (beginning) to t_n (end), M_{CO_2} is the CO_2 molar weight, ρ_{CO_2} is the CO_2 density, G is the gas flow rate, $P^*_{CO_2}$ is the CO_2 partial pressure at the outlet, P_{CO_2} is the CO_2 partial pressure at the inlet, $P_{total}$is the total pressure, and $[\mathrm{CO_2}]_T$ is the total absorbed CO_2 in mole by the liquid phase.

$$[\mathrm{CO_2}]_T = \sum_{i=1}^{n} \frac{1}{2} \times G \times \frac{\rho_{CO_2}}{M_{CO_2}} \left[\frac{\left(P_{CO_2} - P^*_{CO_2}\right)_i + \left(P_{CO_2} - P^*_{CO_2}\right)_{i+1}}{P_{total}} \right] \times [t_{i+1} - t_i] \qquad (2)$$

Fig. 2 depicts a schematic diagram of the reactor with WWC. The reactor's inner diameter is 12.83 cm, and the water bath jacket covers it to maintain the temperature. A thin layer of the liquid wetted the stainless steel column (wetted-wall-column) as the liquid flowed down the column.

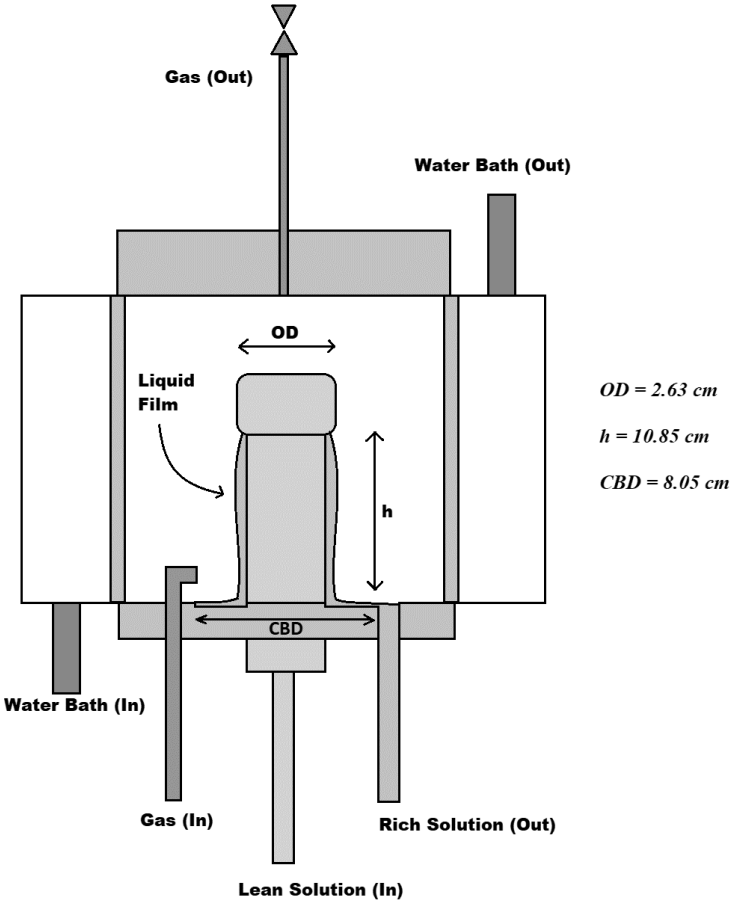

Fig. 2: The schematic diagram of the reactor with WWC.

The gas stream flowed upwards through the reactor, and at this moment, the CO_2 counter-currently contacted the liquid film on the wetted column. While the gas and liquid were interacting, some CO_2 molecules transferred to the liquid phase. The rich solution was withdrawn from the reactor's base, and the gas containing less CO_2 discharged from the top of the reactor. Pacheco [34] measured the properties of the liquid falling film in WWC using the momentum balance. The thickness of the liquid film (δ) can be determined by **Eq. (3)**, where Q_{sol} is the liquid flow rate, μ is the liquid viscosity, W is the wetted perimeter, ρ is the liquid density, and g_c is the gravity constant. A viscometer (Brookfield LV SC4-18) was used to measure the liquid viscosity. **Eq. (4)** gives the superficial velocity (u_s) as a function of film

thickness, gravity constant, liquid density and viscosity. Then the contact time (τ) can be measured by dividing the column's height (contact length) by superficial velocity (**Eq. (5)**).

$$\delta = \sqrt[3]{\frac{3 \times \mu \times Q_{sol}}{W \times g_c \times \rho}} \tag{3}$$

$$u_s = \frac{\delta^2 \times \rho \times g_c}{2\mu} \tag{4}$$

$$\tau = \frac{h}{u_s} \tag{5}$$

According to **Eq. (6)**, the total contact area is measured by aggregating the column's side area and the reactor's wetted-base area. The column's side area can be calculated by **Eq. (7)**, assuming the liquid surface forms a column with a radius of the liquid film thickness (δ) added to the column's radius (*OD/2*). The reactor's wetted-base area is assumed to have a ring shape with a width of ($CBD - (OD + 2\delta)$) according to **Eq. (8)**. Based on these calculations, the total contact area was calculated to be 139.13 cm^2.

$$\text{Contact Area} = \text{Area}_{\text{base}} + \text{Area}_{\text{side}} \tag{6}$$

$$\text{Area}_{\text{side}} = h \times \pi \times (OD + 2\delta) \tag{7}$$

$$\text{Area}_{\text{base}} = \frac{\pi}{4}(CBD^2 - (OD + 2\delta)^2) \tag{8}$$

3 Mass Transfer Calculations

According to the mass transfer definition, CO_2 absorption happens as the CO_2 molecules in the gas side move to the liquid side. The rate of this transition per unit of area is called CO_2 mass flux $\left(N_{CO_2}\right)$ or mass transfer rate per area $[mol/s.m^2]$. Based on the conservation of mass for CO_2, the total CO_2 flux is the same flux in each phase:

$$N_{CO_2} = K_G\left(P_{CO_2,G} - P^*_{CO_2}\right) = k_g\left(P_{CO_2,G} - P_{CO_2,i}\right) = k_l\left(C_{CO_2,i} - C_{CO_2,L}\right) \quad (9)$$

The correlation term with K_G is referred to as the overall mass transfer, in the gas phase, it is named as k_g and in the liquid phase, it is called k_l. **Fig. 3** shows a schematic representation of the mass transfer process. The diagram depicts the mass transfer according to the two-film theory. Per this theory, the mass transfer coefficient is directly proportional to diffusion and inversely proportional to film thickness. In two-film theory, the main mass transfer resistance is assumed to be at a thin layer of two phases interface (film). The CO_2 concentration profile is homogeneous in each phase, and it has a linear profile in the tiny film [35]. The concentration gradient causes CO_2 to move from the bulk gas phase to the bulk liquid phase. In the bulk gas phase, the concentration of CO_2 is considered to be steady at ($P_{CO_2,G}$), and declines linearly to $P_{CO_2,i}$ at the interface. Then the liquid side of the interface takes the CO_2 with a mole fraction of $C_{A,i}$ which reduces to a constant concentration of $C_{CO_2,L}$.

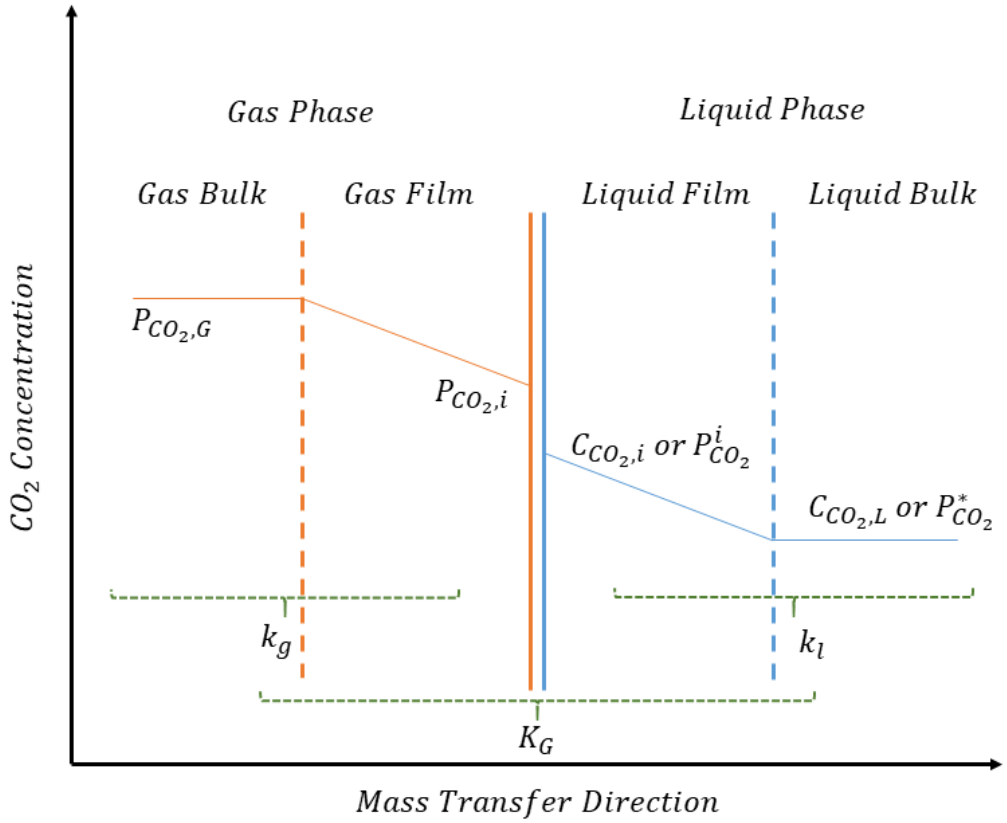

Fig. 3: The mass transfer profile in the two-film theory.

Moreover, it is assumed that the CO_2 is in equilibrium at the interface; therefore, a proportionality factor (Henry's law constant, H_{CO_2}) is added to satisfy the driving force terms. (**Eq. (10)**):

$$N_{CO_2} = \frac{k_l^0}{H_{CO_2}}\left(P_{CO_2,i} - P^*_{CO_2}\right) = k_l\left(C_{CO_2,i} - C_{CO_2,L}\right) \tag{10}$$

Where k_l^0 is the physical mass transfer coefficient. When a chemical reaction occurs together with molecular diffusion, k_l^0 only contributes partially to the liquid side of mass transfer (k_l); thus, a separate parameter is necessary.

3.1 Physical Mass Transfer Coefficient in Liquid phase (k_l^0)

The physical mass transfer coefficient in the liquid side (k_l^0) is significant in the study of mass transfer with chemical reactions. Because the k_l^0 only explains the physical diffusion and finding it can help to find the contribution of chemical reaction to the mass transfer. When only the physical mass transfer is taken into account, k_l^0 and k_l are the same. Pacheco [34] was the first to model and improve the liquid film physical mass transfer coefficient for an amine system in WWC. Pacheco [34] modelled the experimental results with a mathematical model, which was first introduced by Pigford [36]. In this theoretical model, k_l^0 is a function of solution flow rate (Q_{sol}), gas-liquid contact area (A), and a dimensionless driving force Θ (**Eq. (11)**) [29].

$$k_l^0 = \frac{Q_{sol}}{A} \times (1 - \Theta) \tag{11}$$

The dimensionless driving force itself is a function of another dimensionless parameter called penetration distance (η). The dimensionless penetration distance can be calculated by knowing the contact time (τ), the liquid film thickness (δ), and the diffusion coefficient of CO_2 in the liquid phase (D_{CO_2}), according to **Eq. (12)**. The dimensionless driving force is evaluated using two formulas based on penetration distances above 0.01 and below 0.01, see **Eq. (13)** [37].

$$\eta = \frac{D_{CO_2} \times \tau}{\delta^2} \tag{12}$$

$$\Theta = \begin{cases} 1 - 3\sqrt{\frac{\eta}{\pi}} & , \quad \eta < 0.01 \\ 0.018\exp(-204.7\eta) + 0.036\exp(-105.6\eta) \\ +0.1\exp(39.21\eta) + 0.785\exp(-5.121\eta) & , \quad \eta \geq 0.01 \end{cases} \tag{13}$$

3.2 Mass Transfer Coefficient in Gas Phase (k_g)

The mass transfer coefficient in the gas phase (k_g) can be measured using the Sherwood number correlation (**Eq. (14)**). The diffusion coefficient of CO_2 (D_{CO_2}) is the binary diffusion coefficient of CO_2 in N_2 in the gas phase [38]. Pacheco [34] used a model offered by Byers and King [39] (**Eq. (15)**) to find a correlation for the Sherwood number in WWC (**Eq. (16)**). Later, many studies used the same correlation to find k_g. Likewise, this correlation was used in this work since the WWC geometries and condition in both studies are very similar. In **Eq. (15)**, d_h is the hydraulic diameter of WWC (2.61 cm), h is the column's height (10.84 cm), *Sh, Re, Sc* are the Sherwood number, the Reynolds number, and the Schmidt number, respectively. The α and β are the parameters to be found experimentally based on the WWC specifications.

$$Sh = \frac{R \times T \times k_g \times d_h}{D_{CO_2}} \tag{14}$$

$$Sh = \alpha . \left(\frac{Re \times Sc \times d_h}{h}\right)^{\beta} \tag{15}$$

$$Sh = 1.075 \left(\frac{Re \times Sc \times d_h}{h}\right)^{0.85} = 1.075 \left(\frac{d_h^2 \times u_G}{h \times D_{CO_2}}\right)^{0.85} \tag{16}$$

3.3 Overall Mass Transfer Coefficient (K_G)

The difference of CO_2 concentration in the gas phase before and after the reactor gives the CO_2 flux, according to **Eq. (17)**. The total pressure (P_{total}) is atmospheric, and V_m is the ideal gas molar volume. By knowing N_{CO_2}, the overall mass transfer can be calculated according to **Eq. (9)**. When the measured flux is plotted against the logarithmic mean of partial pressure driving force ($N_{CO_2}\ vs.\ \left(P_{CO_2} - P^*_{CO_2}\right)_{LM}$), the slope of the straight line gives the K_G (**Eq. (18)**). Typically, multiple reading points are needed to find the logarithmic mean and the slope (K_G).

$$CO_2 \text{ flux}: N_{CO_2}\left[\frac{\text{mol}}{\text{s. cm}^2}\right] = \frac{\left(P_{CO_2} - P^*_{CO_2}\right)_i}{P_{\text{total}}} \times G \times \frac{1}{V_m \times A} \tag{17}$$

$$N_{CO_2} = K_G \times \left(P_{CO_2} - P^*_{CO_2}\right)_{LM} \tag{18}$$

The **Eq. (19)** gives the $\left(P_{CO_2} - P^*_{CO_2}\right)_{LM}$ as follows:

$$\left(P_{CO_2} - P^*_{CO_2}\right)_{LM} = \frac{\left(P_{CO_2} - P^*_{CO_2}\right)_i - \left(P_{CO_2} - P^*_{CO_2}\right)_{i+1}}{\ln\left(\frac{\left(P_{CO_2} - P^*_{CO_2}\right)_i}{\left(P_{CO_2} - P^*_{CO_2}\right)_{i+1}}\right)} \tag{19}$$

3.4 Total Mass Transfer Coefficient in Liquid Phase (k'_g)

The absorption of CO_2 in an amine system involves a series of chemical reactions. The rate of mass transfer can be accelerated by chemical reactions between gas species and liquid components. The enhancement factor, E, can explain this acceleration. Therefore, the enhancement factor changes **Eq. (10)** to **Eq. (20)**:

$$N_A = \frac{E \times k_l^0}{H_{CO_2}}\left(P_{CO_2,i} - P^*_{CO_2}\right) = k'_g\left(P_{CO_2,i} - P^*_{CO_2}\right) \tag{20}$$

The factor behind the $\left(P_{CO_2,i} - P^*_{CO_2}\right)$ in **Eq. (20)** is called total mass transfer coefficient in the liquid phase (k'_g), and the unit is $[mol/Pa.s.m^2]$.

Also, since the mass transfer resistance is the inverse of the mass transfer coefficient, the overall mass transfer resistance ($1/K_G$) is the sum of the liquid-side resistance (H/k_l) and the gas-side resistance ($1/k_g$), see **Eq. (21)**. On the other hand, the total mass transfer is either controlled by liquid-phase or gas-phase or even both. Therefore, depending on which resistance is dominant and which one is negligible, the total mass transfer parameter is evaluated [40].

$$\frac{1}{K_G} = \frac{1}{k_g} + \frac{1}{k_g'} \tag{21}$$

In **Eq. (21)**, the overall and the gas-side mass transfer coefficients are already known by **Eqs. (18, 15)**, respectively. Thus, the total mass transfer coefficient in the liquid phase (k_g') can be measured by **Eq. (21)**. It should be noted that when dealing with chemical absorption, the common standard symbol to show the mass transfer coefficient in the liquid phase is k_g' [41].

4 Results and Discussion

In this study, the mass transfer coefficients of CO_2 in the aqueous MEA solution mixed with varying glycerol concentrations were measured at 313 K, 323 K and 333 K in the WWC. The MEA mass fraction was set at 25 wt%, which is 5% less than the composition used in the industrial application (MEA 30 wt%), and the glycerol concentration was ranged from 5 to 20 wt%. To ensure the precision of measurements, a set of experiments of overall mass transfer coefficient using the 25 wt% MEA and 10 wt% glycerol was replicated three times at 333 K to obtain the margin of error. The margin of error for the overall mass transfer coefficient was ±5%.

This section represents the experimental results of mass transfer coefficients of CO_2 absorbing into the aqueous MEA-glycerol solution at mentioned temperatures and ambient pressure. The results are described below.

4.1 Physical Mass Transfer Coefficient (k_l^0)

For each temperature and glycerol concentration, the η, Θ, and consequently the k_l^0 were determined using **Eqs. (11, 12, 13)** and then the k_l^0 plotted as shown in **Fig. 4**. The graph depicts that increasing the glycerol composition decreased the k_l^0, and the k_l^0 is higher at elevated temperatures. Because the CO_2 absorption in glycerol is mainly a physical absorption, the dependency of k_l^0 to glycerol composition might be due to the viscosity since the higher

viscosity drops the molecular diffusion significantly. At 333 K, the physical mass transfer of CO_2 molecules into the solution increased considerably, compared with a modest increase from 313 K to 323 K. **Table 1** shows the detailed information of k_l^0. As shown, the 20G25M solution at 313 K has the lowest k_l^0, while the 5G25M at 333 K has the highest. In another study by Dugas and Rochelle [29], the k_l^0 for CO_2 into a 7m MEA solution (30 wt% MEA) at 313 K and 333 K were reported to be 6.5×10^{-3} cm/s and 7.9×10^{-3} cm/s, respectively. The experimental conditions of their work were slightly different from this study, such as the contact area was smaller (38.53 cm^2), and the liquid flow rate was lower (3.1 ml/s). However, the value of k_l^0 for both studies are in fair agreement.

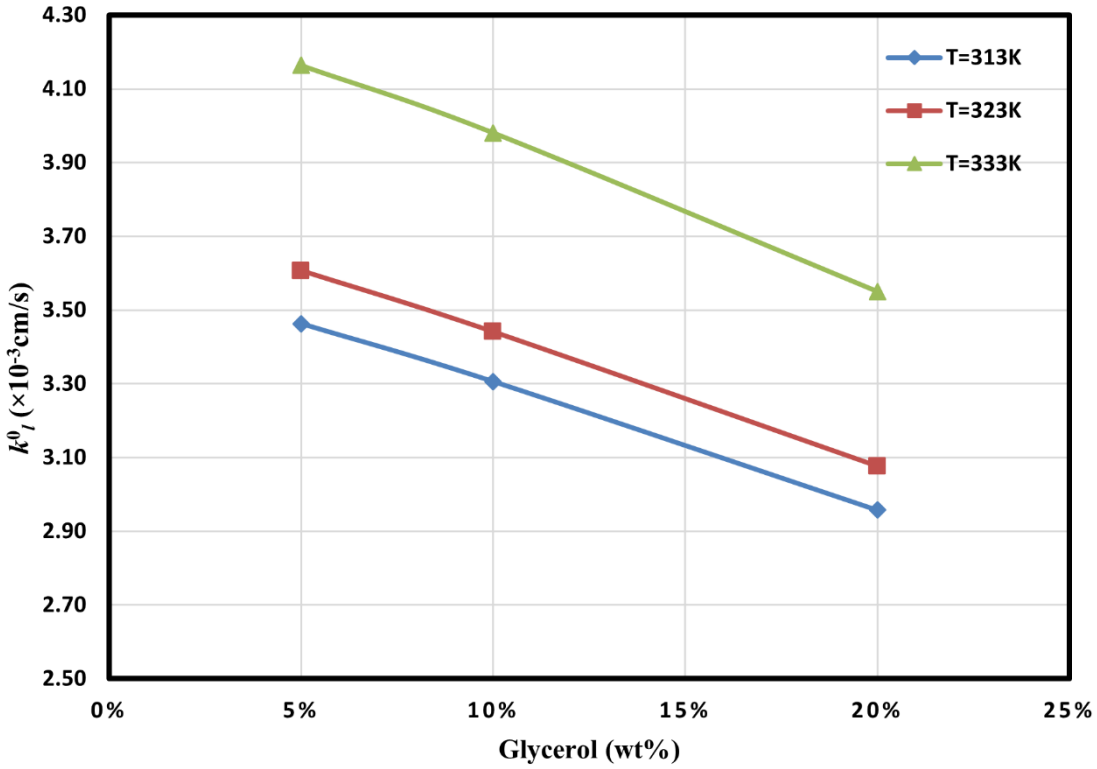

Fig. 4: The k_l^0 at three glycerol compositions and temperatures.

Table 1: The detailed k_l^0 of CO_2 for the aqueous MEA-glycerol solution.

Glycerol wt%	T (K)	Contact area (cm^2)	Q_{sol} (ml/s)	η	Θ	k_l^0 ($\times 10^{-3}$ cm/s)
5		139.1	25	1.30×10^{-4}	0.9807	3.463
10	313	139.2	25	1.18×10^{-4}	0.9815	3.306
20		139.6	25	9.53×10^{-5}	0.9834	2.957
5		138.9	25	1.40×10^{-4}	0.9799	3.607
10	323	139.1	25	1.28×10^{-4}	0.9808	3.441
20		139.4	25	1.03×10^{-4}	0.9828	3.077
5		138.5	25	1.86×10^{-4}	0.9769	4.163
10	333	138.6	25	1.70×10^{-4}	0.9779	3.980
20		139.0	25	1.36×10^{-4}	0.9802	3.550

4.2 Gas-Side Mass Transfer Coefficient (k_g)

The mass transfer coefficient in the gas phase (k_g) is calculated using **Eq. (16)**, and the results are listed in **Table 2**. As shown, the glycerol composition does not affect the k_g, while the temperature has a small effect on the k_g. As listed in **Table 2**, the k_g at 333 K is the lowest ($1.55\times10^{-9}\ mol/Pa.s.cm^2$) compared with the k_g at 313 K, which is the highest ($1.61\times10^{-9}\ mol/Pa.s.cm^2$). There is a slight difference between these two values, which shows that the effect of temperature is negligible. The magnitude ratio of k_g to K_G indicates that the mass transfer resistance in the gas phase ($1/k_g$) is negligible compared with the total mass transfer resistance. On the other hand, the mass transfer is controlled by the liquid phase. The negligible mass transfer resistance in the gas phase also shows that the wetted column is well built to provide a completely wetted surface of falling film liquid [34].

Table 2: The detailed k_g of CO_2 in the wetted-wall column

Glycerol wt%	Temp. (K)	d_{wwc} (cm)	u_G (cm/s)	G(ml/s)	h_{wwc} (cm)	Sherwood	D_{CO2-N2} (cm^2/s)	k_g (mol/cm^2.Pa.s)
5	313	2.63	33.12	16.65	10.85	63.874	0.1729	1.614×10^{-9}
10								
20								
5	323	2.63	33.15	16.66	10.85	59.464	0.1881	1.584×10^{-9}
10								
20								
5	333	2.63	33.17	16.67	10.85	55.667	0.2033	1.554×10^{-9}
10								
20								

4.3 Overall Mass Transfer Coefficient (K_G)

As mentioned, the graph's slope of CO_2 flux over the logarithmic mean of partial pressure gives the overall mass transfer coefficient (K_G). As a result, the total liquid phase mass transfer (k_g') can be calculated by knowing K_G and k_g. As an example of the measurement process, **Fig. 5** displays a plot for the 10G25M solution at 333 K. **Table 3** contains all the data for the overall mass transfer coefficient.

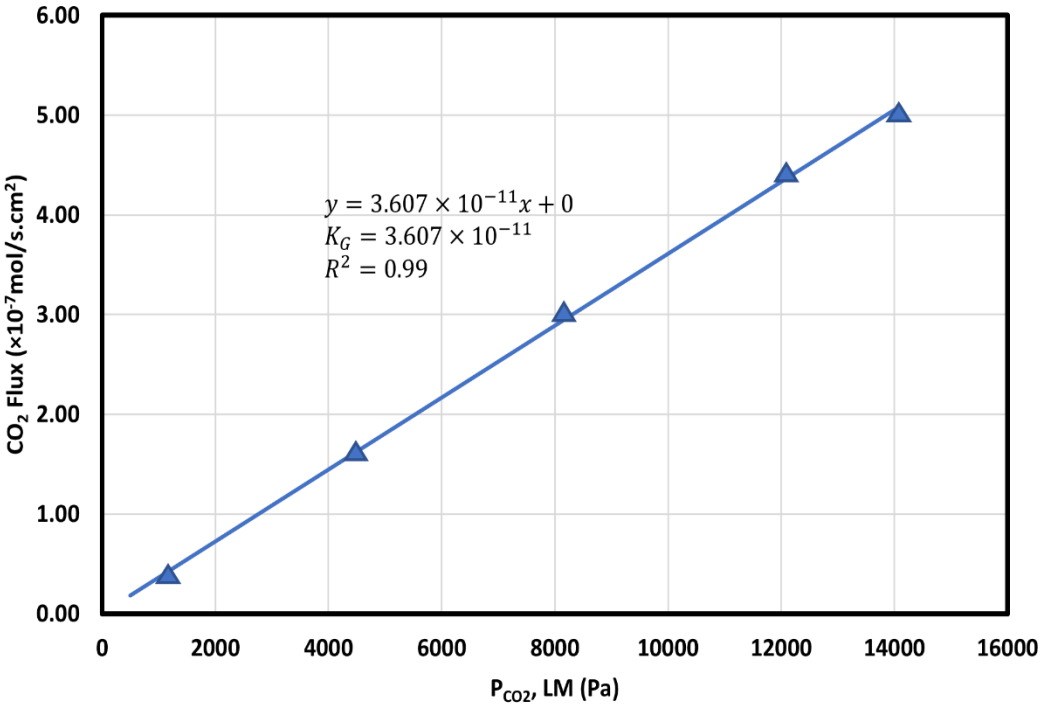

Fig. 5: The K_G calculation using flux's slope versus the logarithmic mean of partial pressure for 10G25M solution at 333 K

Table 3 shows that the 10G25M solution has the maximum K_G value at all three temperatures. Since the gas-side mass transfer is not dependent on glycerol concentration, the changes in K_G is due to the changes in liquid-side mass transfer, which is dependent on the liquid composition. There is no reported data for the same solution as this work in the literature. However, in a few studies, researchers investigated the K_G for CO_2 in 7m MEA. Puxty et al. [28] and Han et al. [42] reported K_G for CO_2 in the 7m MEA solution at 313 K to be 2.80×10^{-10} $(mol/Pa.s.cm^2)$ and 1.12×10^{-10} $(mol/Pa.s.cm^2)$, respectively. Karlsson et al. [41] also reported the K_G for CO_2 in the same solution at 300 K to be 1.7×10^{-10} $(mol/Pa.s.cm^2)$. Compared with these studies, the K_G of this work is almost 5 times smaller than K_G for CO_2 in 7m MEA.

Table 3: Overall mass transfer coefficient (K_G) for three solutions at three temperatures.

Glycerol wt%	Temp. (K)	V_m (L/mol)	P_{total} (atm)	P_{CO2} (kPa)	G (ml/min)	Contact area (cm^2)	K_G ($mol/cm^2.Pa.s$)
5			1	15	996	139.1	3.460×10^{-11}
10	333	27.3	1	14.5	999	139.2	3.607×10^{-11}
20			1	14.8	1002	139.7	3.166×10^{-11}
5			1	14.9	997	138.9	2.998×10^{-11}
10	323	26.55	1	15	1000	139.1	3.088×10^{-11}
20			1	15	1002	139.5	2.780×10^{-11}
5			1	14.7	1000	138.4	2.662×10^{-11}
10	313	25.66	1	14.9	1001	138.6	2.789×10^{-11}
20			1	15	999	139.0	2.402×10^{-11}

4.4 Total Liquid-Side Mass Transfer Coefficient (k'_g)

In this study, the CO_2 mass transfer coefficient in the liquid phase (k'_g) and the CO_2 loading (α_{CO_2}) over the CO_2 dynamic quasi-equilibrium partial pressure ($P^*_{CO_2}$) were determined. Over time, the absorbed CO_2 increased in the solvent. However, since each run for the absorption process in WWC is very slow, and the system is a semi-batch process, the gas and liquid at each reading point were approximately in equilibrium; therefore, the CO_2 loading and the partial pressure of CO_2 were in the quasi-equilibrium state. As mentioned before, the experimental measurements and calculations were adopted from similar works by Yuan et al. [43], Song [44], and Li et al. [31], which have a fair agreement with packing columns to scale-up [45]. Due to the k'_g expressing both the chemical and physical transfer rate, it can also be considered as the absorption rate. **Fig. 6-8** show the k'_g versus CO_2 partial pressure at three temperatures for the 20G25M, 10G25M, and 5G25M solution, respectively. As shown in **Fig. 6**, the absorption rate (k'_g) for the 20G25M at 323 K and 333 K are very close to each other, while at 313 K is slightly dropped. In other words, lower temperature leads to lower absorption rate in solutions with 20 wt% glycerol.

The absorption rate or k_g' of CO_2 into the 10G25M and 5G25M are plotted in **Fig. 7 and 8**. In both graphs, as the temperature dropped, the k_g' in the solutions decreased correspondingly as expected according to the Arrhenius equation. Comparing the k_g' of three solutions at all temperatures shows that the solution containing 10 wt% glycerol has the highest k_g'. The difference in k_g' between 10G25M and 20G25M might be due to the lower viscosity of the 10G25M than 20G25M. This can be explained by the fact that the CO_2 diffusivity is higher in a solution with lower viscosity. However, the scenario for 5G25M is not the same. Although the 10G25M has a higher viscosity than the 5G25M, the k_g' in the 5G25M is slightly lower than 10G25M. This could be mainly due to the more chemical and electrostatic interactions between the CO_2 and glycerol molecules in 10G25M, accelerating the absorption rate. The structure of the glycerol molecules has three high polar OH groups with less polar C-H bonds. Although the CO_2 is a non-polar molecule, each C-O bond has a polarity, which interacts with the OH groups in glycerol. The more glycerol molecules in 10G25M than 5G25M, the more interaction and the higher k_g' consequently. A similar justification has been given by Song and Rochelle [26], saying strong electron interactions are between the polar C-O bonds in CO_2 and hydroxyl groups (OH) in the solution. Moreover, the absorption could be increased because the OH group has a high affinity for the CO_2 molecules [12].

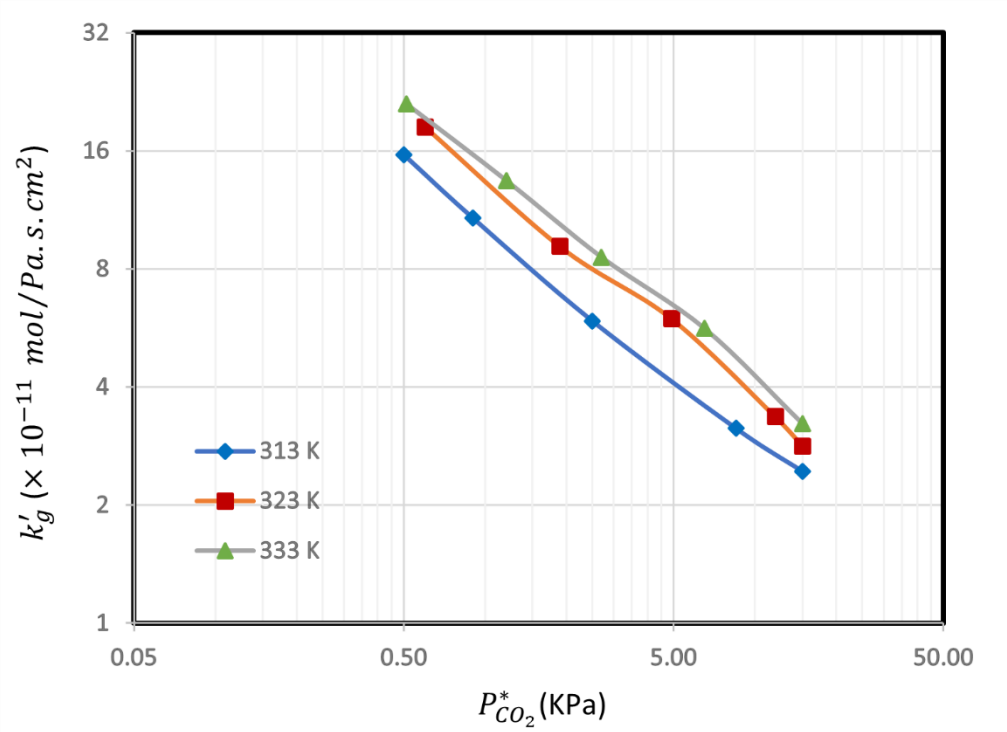

Fig. 6: The k'_g versus $P^*_{CO_2}$ at 313 K, 323 K, and 333 K for the 20G25M.

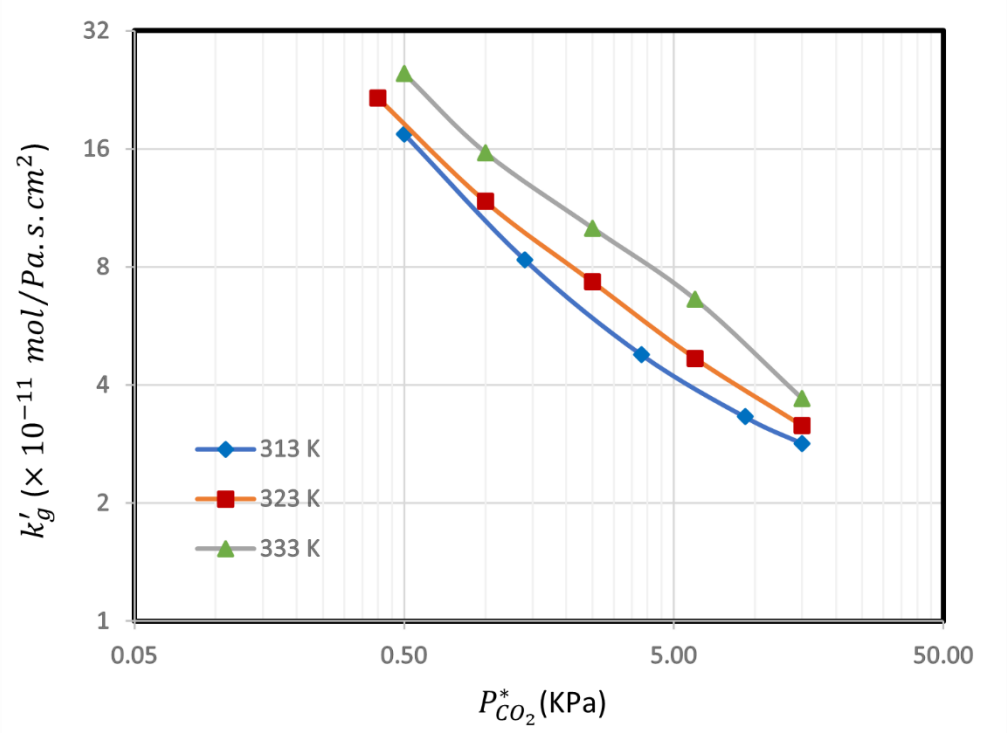

Fig. 7: The k'_g versus $P^*_{CO_2}$ at 313 K, 323 K, and 333 K for the 10G25M.

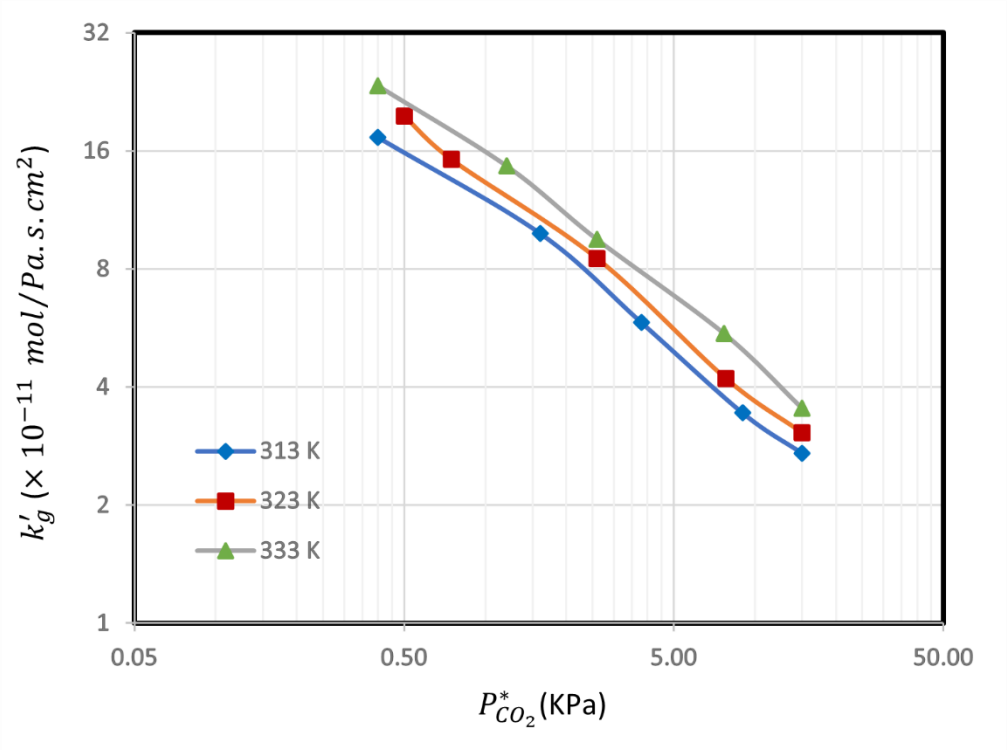

Fig. 8: The k'_g versus $P^*_{CO_2}$ at 313 K, 323 K, and 333 K for the 5G25M.

Fig. 9-11 show the CO_2 quasi-equilibrium loading for the three solutions at temperatures ranging from 313 to 333 K and CO_2 partial pressures ranging from 0.5 to 15 kPa. As shown in the graphs, the uptaken CO_2 into the solution increased when the temperature decreased at the same $P^*_{CO_2}$ for all three solutions. This trend is attributed to the undesirable effect of the temperature rising on an exothermic reaction like amine-CO_2. Also, the absorbed CO_2 increased while the CO_2 partial pressure increased at a constant temperature for all three solutions. This observation was expected because the higher pressure of CO_2 above the solution's surface leads to more CO_2 being absorbed in the solution. In total, temperature and pressure effects have been consistent with the general trend of CO_2 absorption in an amine-based solution [12, 46, 47].

Comparing the solutions, the 10G25M showed the highest loading, followed by 5G25M and 20G25M. For example, the CO_2 loading for 5G25M, 10G25M and 20G25M at 313 K and 15 kPa were 0.56, 0.575 and 0.51 ($mol\ CO_2/\ mol\ Alk$), respectively. Considering the CO_2 loading

in 10G25M and 5G25M reveals that adding glycerol improved the loading slightly. This could be due to the fact that glycerol is a better physical absorbent for CO_2 than water [12]. Therefore, increasing glycerol from 5 wt% to 10 wt% leads to increased CO_2 absorption. However, as the glycerol concentration reaches 20 wt%, the CO_2 absorption drops notably. This phenomenon is mainly related to the water content of the solution. Since the glycerol content in the solution has been increased, the water-to-MEA ratio decreased. According to the Zwitterion mechanism, which explains the reaction between CO_2 and aqueous amines, the H_2O molecules contribute significantly to the deprotonation of Zwitterion. The more deprotonated Zwitterion, the more CO_2 reacts with MEA, and eventually, the more CO_2 loading [48]. Overall, the addition of glycerol up to 10 wt% could improve the absorption rate (k_g') and the CO_2 loading (α_{CO_2}) at the atmospheric pressure and temperatures ranging from 313 to 333 K.

Another feature, which can be analysed throughout the CO_2 loading's graphs, is the CO_2 cyclic capacity (ΔC). The CO_2 cyclic capacity means the total loaded CO_2 per total solution's mass at each absorption cycle. Mathematically it is determined by measuring the slope of the CO_2 loading graph according to **Eq. (22)** [43]:

$$\Delta C = (\alpha_{rich} - \alpha_{lean}) \times (\text{mol Alk})/\text{total mass} \quad (22)$$

The α_{rich} is the final CO_2 loading at 15 kPa, and the α_{lean} is the initial CO_2 loading at 0.5 kPa. If the solution has a high ΔC , it means that for absorbing a specific amount of CO_2 less amount of solvent is required. This could affect the energy needed for pumps and heat exchangers and the regeneration costs [37]. As shown in **Fig. 9-11**, all graphs have approximately the same slope for each solution at three different temperatures, meaning that temperature has no significant effect on the ΔC for all solutions. Moreover, it can be concluded that the addition of 5-20 wt% glycerol to the aqueous MEA solution would maintain the CO_2 cyclic capacity over the investigated range of temperature.

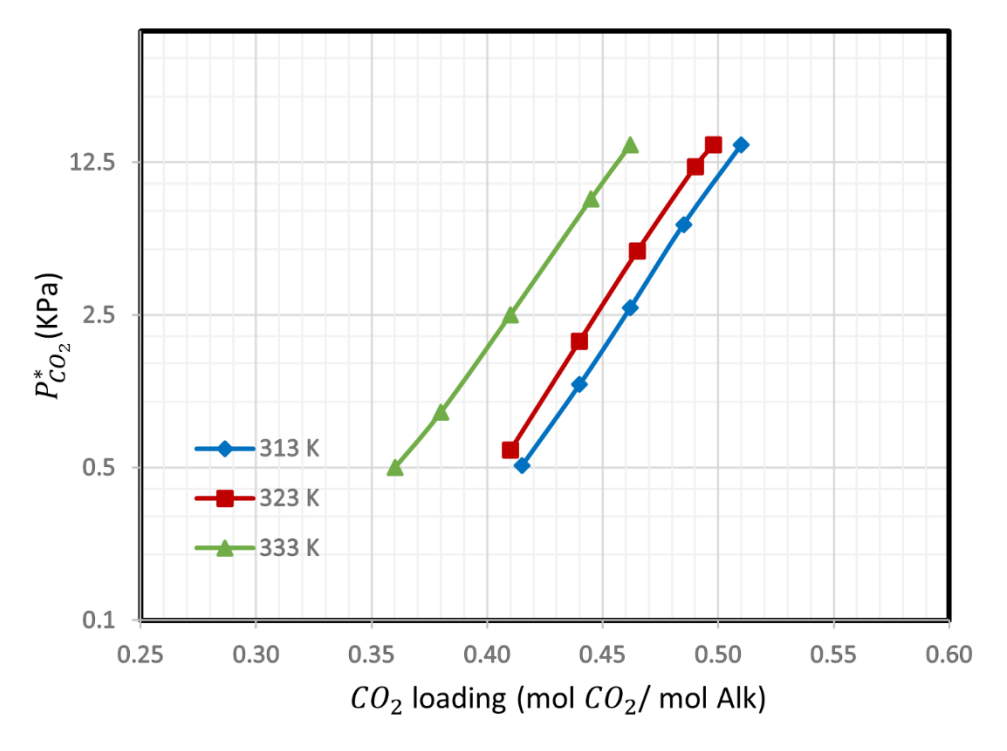

Fig. 9: $P^*_{CO_2}$ versus CO_2 loading at 313 K, 323 K, and 333 K for the 20G25M.

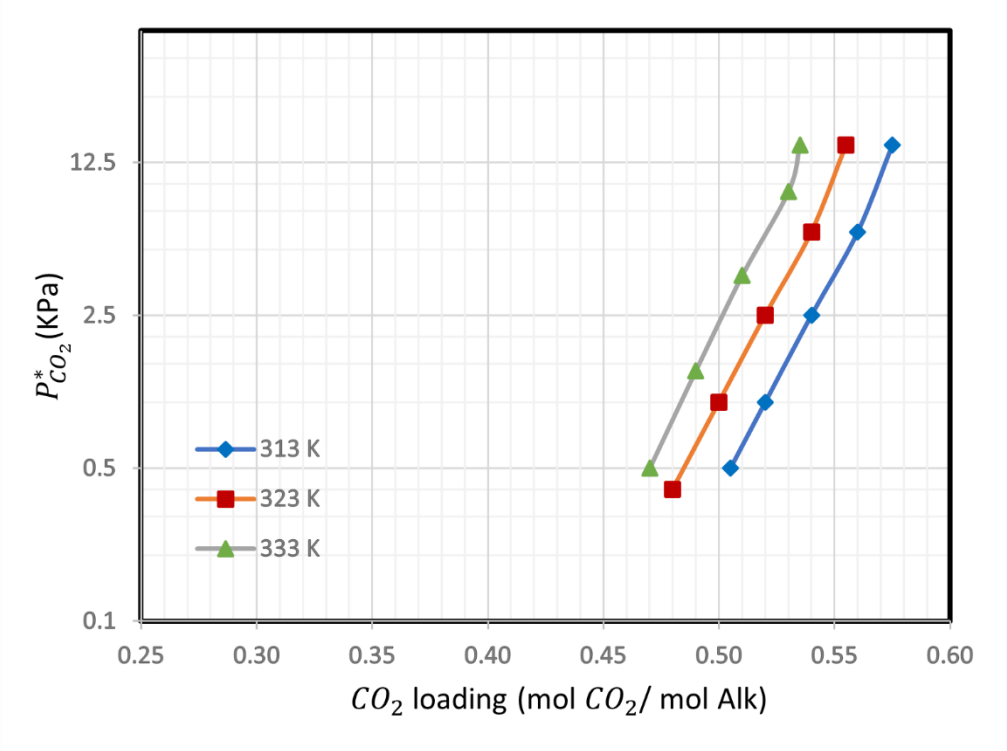

Fig. 10: $P^*_{CO_2}$ versus CO_2 loading at 313 K, 323 K, and 333 K for the 10G25M.

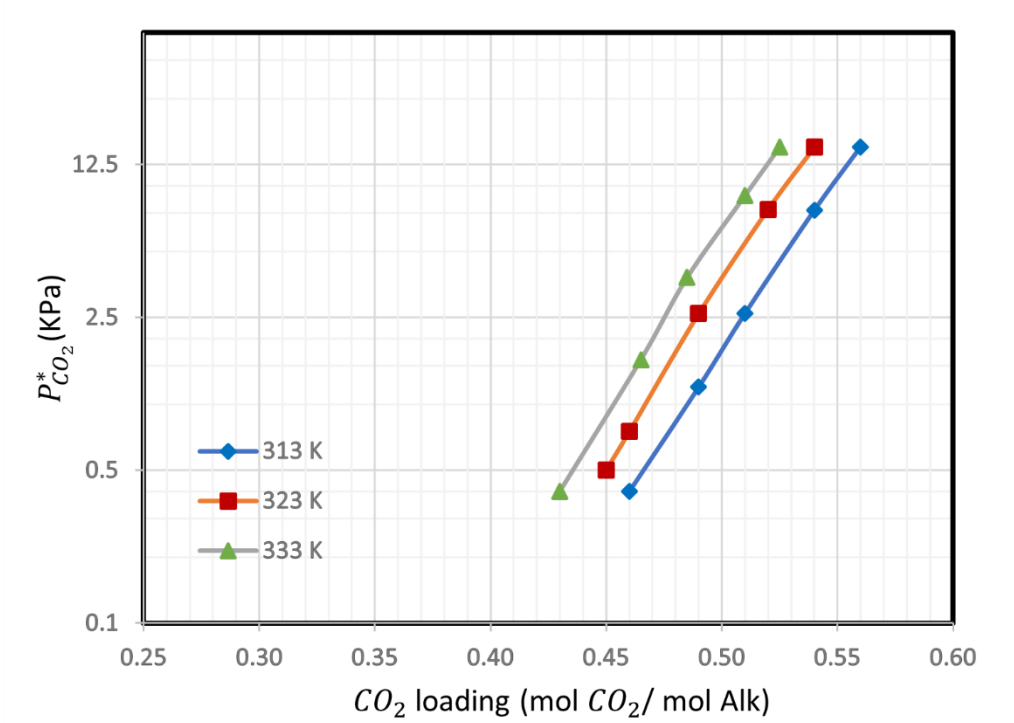

Fig. 11: $P^*_{CO_2}$ versus CO_2 loading at 313 K, 323 K, and 333 K for the 5G25M.

4.5 Comparison of (k'_g) in This Work and Literature

Fig. 12 and 13 demonstrate the k'_g at 313 and 333 K respectively for the 10G25M solution, and a few other solutions were investigated in the literature. The solution 10G25M has been selected to compare with the literature data because it showed a better absorption rate and CO_2 loading among the other two solutions. The other solutions from the literature are either conventional solvents or semi-aqueous solvents since they are very comparable to this study. **Fig. 12** shows the k'_g for 10G25M and the other mixtures over various CO_2 partial pressure range at 313 K.

Yuan and Rochelle [30] studied different semi-aqueous amines such as N-methyl-2pyrrolidone (NMP) in a 7m aqueous MEA solution (30 wt% MEA). The k'_g of three mixtures of NMP at 313K are plotted in **Fig. 12**. The plot shows that the k'_g for the 10G25M in lean conditions ($P^*_{CO_2}$ is about 0.5 kPa) was about 40% higher than 7m MEA in 3-water/1-NMP and then gradually converged at higher partial pressures. However, the k'_g for the other two mixtures of

NMP (7m MEA in 1-water/3-NMP and 7m MEA in 1-water/19-NMP) are considerably higher than 10G25M in a wide range of pressure. These mixtures' absorption rates converge only in rich conditions ($P^*_{CO_2}$ is about 5 kPa above).

Fig. 12 also shows k'_g of 7m MEA (30 wt%) measured by Dugas and Rochelle [29]. The measurement has been done in a very similar condition and equipment to this work. The graph allows a direct comparison of the k'_g between 10G25M and the aqueous MEA 30 wt%. As shown, The k'_g of 10G25M is higher than 30 wt% MEA, although it has less MEA in the solution. The difference is remarkable in lean conditions, and k'_g of 10G25M is more than two times of MEA 30 wt%. At higher partial pressure, the gap decreased but still displayed a moderate difference. This trend is roughly the same for the other solutions of 30 wt% MEA+20 wt% MDEA studied by Li [37].

In the range of 0.5 kPa to 5 kPa at 313 K, 7m MEA in 1-water/19-NMP shows the highest k'_g, followed by 7m MEA in 1-water/3-NMP, 4m 2MPZ, 2m 2MPZ, 7m MEA+2m PZ, this work (10G25M), 7m MEA in 3-water/1-NMP and 7m MEA (30 wt% MEA), which show lower coefficient respectively, and 30 wt% MEA+20 wt% MDEA with the lowest k'_g. In addition to CO_2 physical solubility, the catalytic effect of glycerol on CO_2-H_2O solution and glyceroxide formation is a theory to explain the increase in k'_g [26].

Fig. 13 depicts similar graphs for k'_g of various solvents at 333 K. Comparing with **Fig. 12**, generally, the k'_g increased with temperature rise according to the Arrhenius equation. The graphs show an almost similar trend observed at 313 K. The only noticeable difference is the k'_g of 7m MEA in rich conditions ($P^*_{CO_2}$ around 5 kPa) is now closer to the k'_g of this work's solution (10G25M). It means that the temperature increment had a more positive effect on the solution of 7m MEA. On the other hand, according to the Arrhenius equation, the activation energy required for the 7m MEA solution is less than the 10G25M solution. Among all solution

at 333 K and a partial pressure range of 0.5 kPa to 5 kPa, 4m 2MPZ showed the highest k'_g, followed by 7m MEA+2m PZ, this work (10G25M) and 7m MEA, and 30 wt% MEA+20 wt% MDEA with the lowest k'_g.

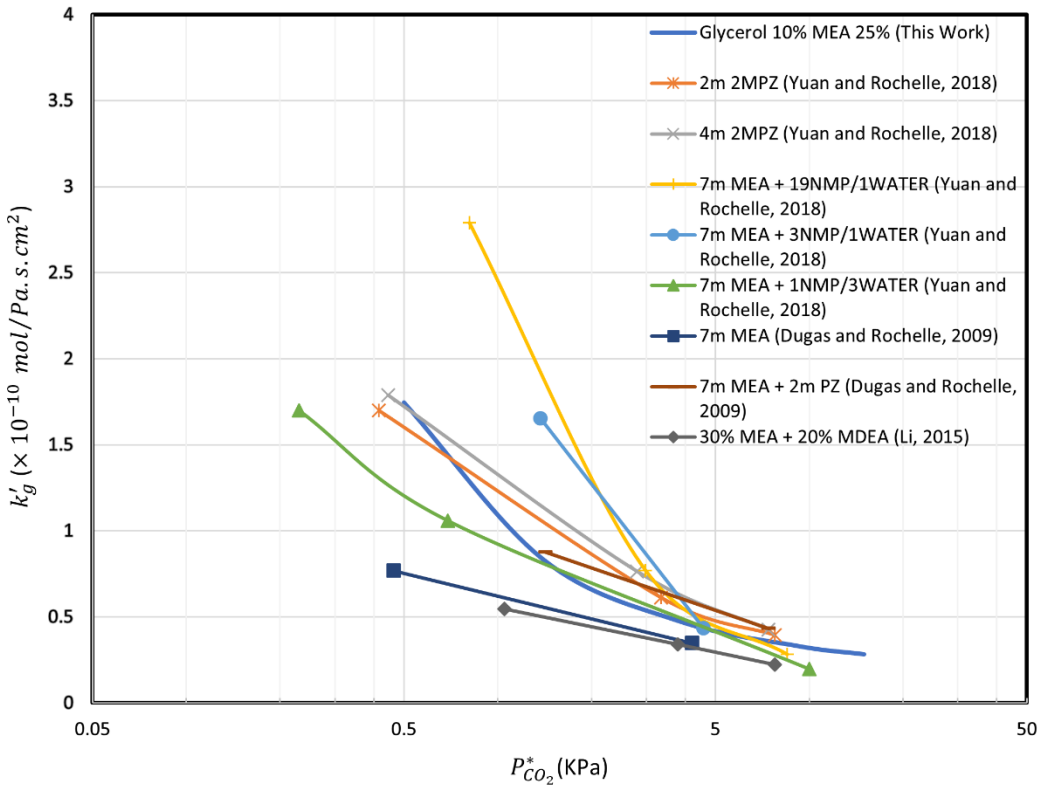

Figure 12: The k'_g versus $P^*_{CO_2}$ at 313 K for the 10G25M and other solutions.

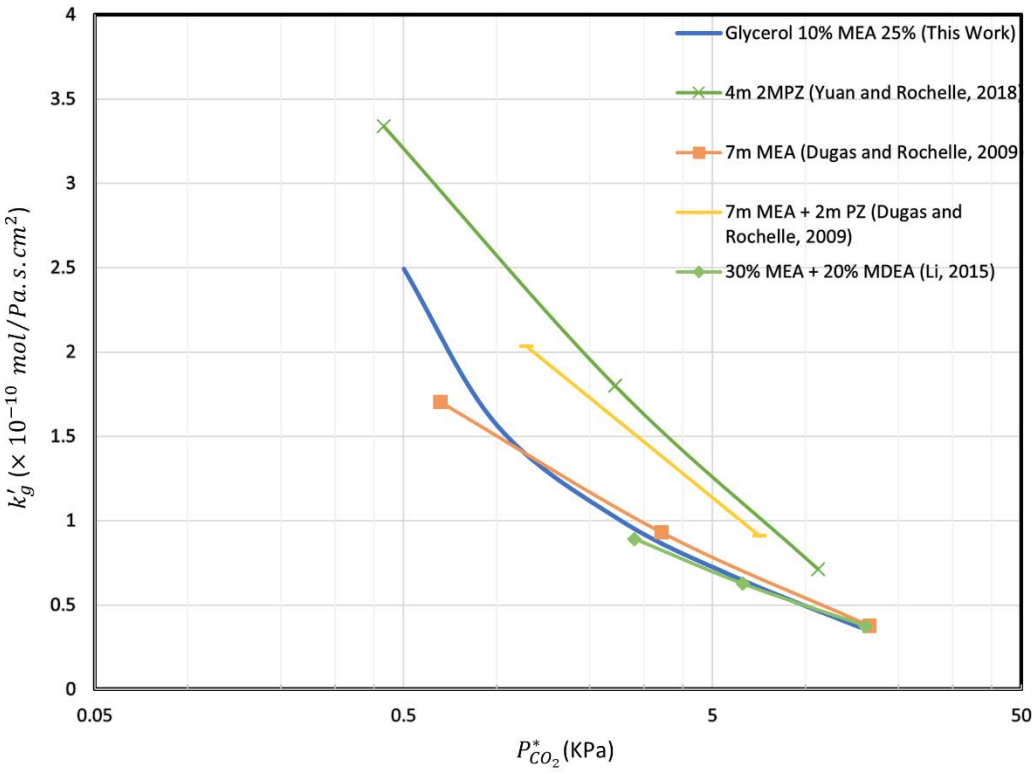

Figure 13: The k'_g versus $P^*_{CO_2}$ at 333 K for the 10G25M and other solutions.

Fig. 14 and 15 show the CO_2 loading of the different solutions over a range of CO_2 partial pressure of 0.2-15 kPa at 313 K and 333 K, respectively. This work's solution (10G25M) showed higher CO_2 loading within the pressure range in both diagrams. However, in terms of CO_2 cyclic capacity, the 10G25M solution has a steeper slope and, eventually, less cyclic capacity than other solutions. This could result from the alkalinity of the 10G25M solution that is weaker than the other investigated solutions. Moreover, the solution's total molecular weight is high, which reduce the total capacity of CO_2. The measured values of absorption rate (k'_g) and CO_2 loading of the aqueous MEA-glycerol solutions studied in WWC are given in **Table 4**.

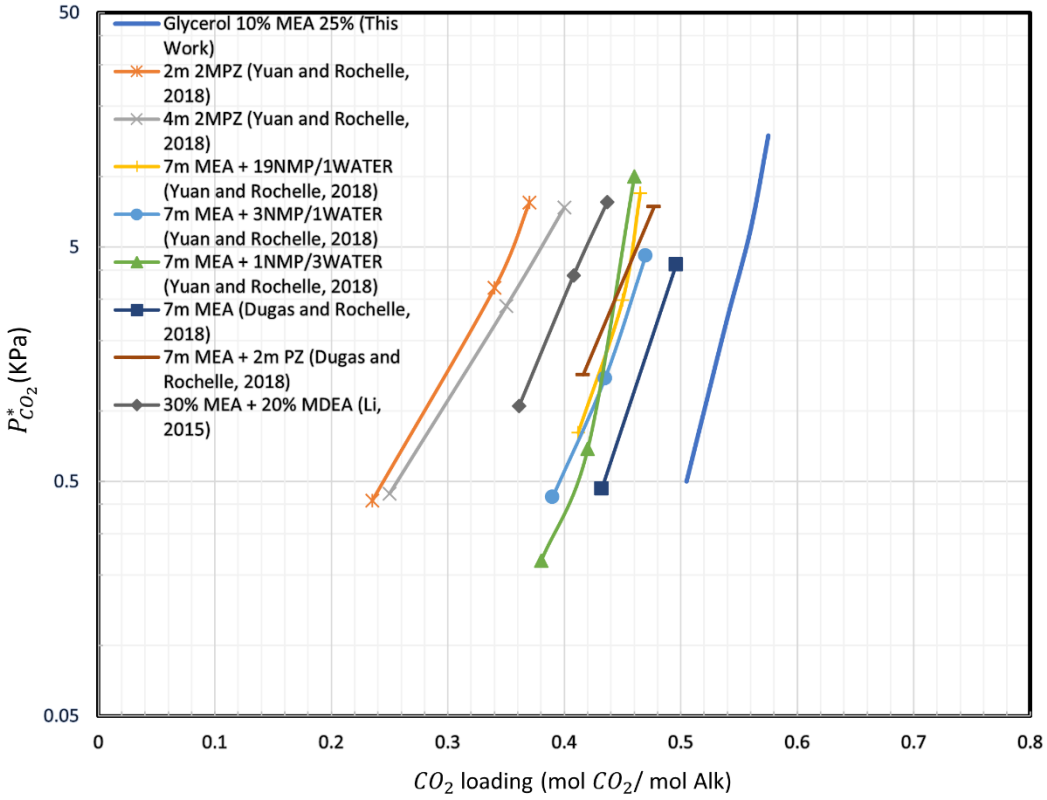

Fig. 14: CO_2 loading of this work's solution and other solutions at 313 K by WWC.

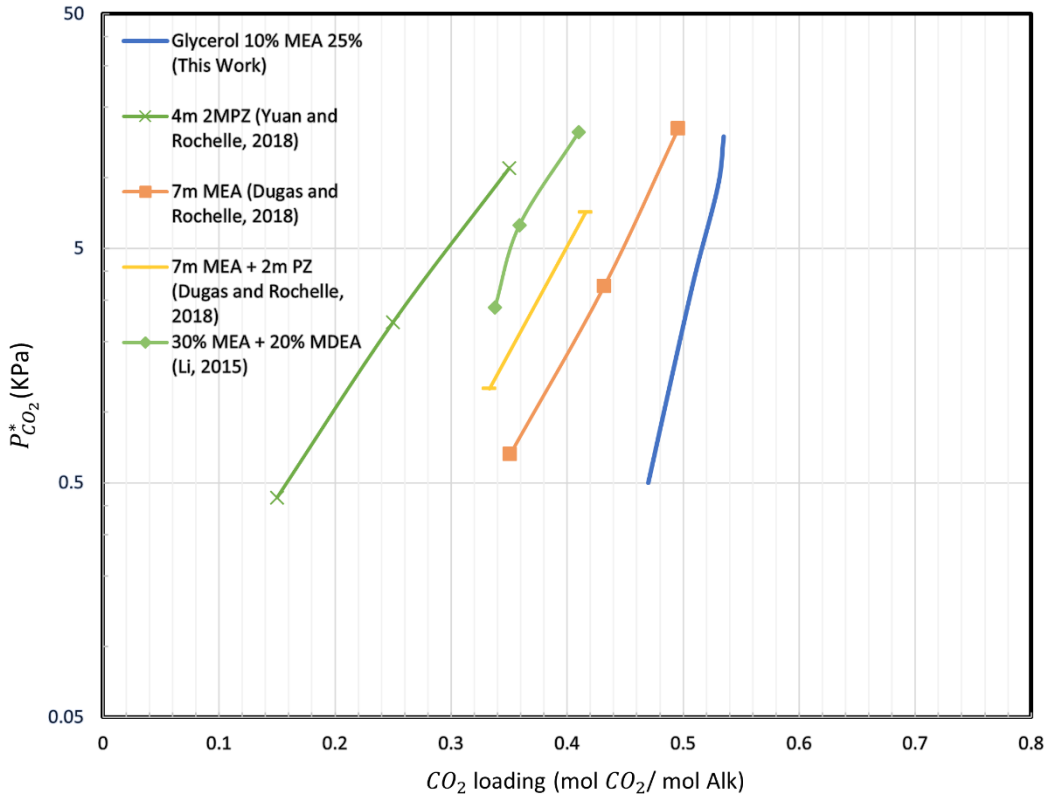

Fig. 15: CO_2 loading of this work's solution and other solutions at 333 K by WWC.

Table 4: WWC measurements of α_{CO_2} and k'_g for three types of aqueous MEA solutions with glycerol.

T (K)	Solution	α_{CO_2} $(mol\ CO_2/\ mol\ Alk)$	P^*_{CO2} (kPa)	$k'_g(\times 10^{-11}\ mol/Pa.s.cm^2)$
313	5G25M	0.462	0.4	17.33
313	5G25M	0.494	1.6	9.86
313	5G25M	0.515	3.8	5.84
313	5G25M	0.542	9	3.43
313	5G25M	0.561	15	2.70
323	5G25M	0.453	0.5	19.64
323	5G25M	0.462	0.75	15.21
323	5G25M	0.494	2.6	8.51
323	5G25M	0.523	7.8	4.21
323	5G25M	0.542	15	3.05
333	5G25M	0.432	0.4	23.44
333	5G25M	0.465	1.2	14.66
333	5G25M	0.485	2.6	9.52
333	5G25M	0.511	7.7	5.48
333	5G25M	0.525	15	3.53
313	10G25M	0.505	0.5	17.47
313	10G25M	0.524	1.4	8.35
313	10G25M	0.546	3.8	4.78
313	10G25M	0.563	9.2	3.32
313	10G25M	0.575	15	2.84
323	10G25M	0.481	0.4	21.58
323	10G25M	0.502	1	11.76
323	10G25M	0.521	2.5	7.33
323	10G25M	0.542	6	4.68
323	10G25M	0.555	15	3.15
333	10G25M	0.471	0.5	24.91
333	10G25M	0.492	1	15.66
333	10G25M	0.511	2.5	10.05
333	10G25M	0.533	6	6.62
333	10G25M	0.535	15	3.69
313	10G25M	0.415	0.5	15.62
313	10G25M	0.443	0.9	10.79
313	10G25M	0.462	2.5	5.89
313	10G25M	0.485	8.5	3.14
313	10G25M	0.512	15	2.44
323	10G25M	0.411	0.6	18.43
323	10G25M	0.441	1.9	9.12
323	10G25M	0.465	4.9	5.98
323	10G25M	0.493	11.9	3.36
323	10G25M	0.498	15	2.83
333	10G25M	0.361	0.51	21.12
333	10G25M	0.382	1.2	13.45
333	10G25M	0.411	2.7	8.58
333	10G25M	0.445	6.5	5.65
333	10G25M	0.462	15	3.23

5 Conclusion

In this study, glycerol as a novel and green solvent was added to the conventional MEA solution to investigate the absorption of CO_2 and mass transfer properties of the system. The experimental work was performed in the wetted-wall column (WWC) to facilitate the mass transfer parameters calculations. Three different aqueous solutions with 25 wt% MEA mixed with 5, 10 and 20 wt% glycerol were prepared. The physical mass transfer coefficient (k_l^0) was obtained according to the theoretical model. The results showed the dependency of physical mass transfer to the temperature and glycerol content of the solution. The highest value of k_l^0 belonged to the solution of 5% glycerol at 333 K, and the lowest one referred to the solution of 20 wt% glycerol at 313 K. The gas-side mass transfer coefficient (k_g) values showed that k_g is a function of gas properties such as flow rate, density, and temperature. In general, the gas phase's mass transfer resistance was found negligible compared to the overall mass transfer resistance. The liquid-side mass transfer coefficient (k_g') and the CO_2 quasi-equilibrium loading were obtained over the CO_2 partial pressure at 313-333 K. The k_g' was calculated by subtracting the gas film resistance ($1/k_g$) from the overall resistance ($1/K_G$), which was calculated as a function of CO_2 flux and CO_2 partial pressure. The results showed the k_g' of the 10G25M solution was higher than the other two solutions. Hence, there are various interactions in the CO_2/MEA/H_2O/glycerol system. There are some adverse effects of adding glycerol on absorption rates, such as high viscosity, and some positive effects, such as molecular interaction between glycerol and CO_2. Also, the results show that the k_g' increased at elevated temperatures, although this dependency was small. Compared to other studies, it was found that the solution with 10 wt% glycerol and 25 wt% MEA could give a significantly high absorption rate. The absorption rate of this solution was at least two times greater than the solution of 30 wt% MEA. It is a remarkable achievement, as the 10G25M solution has 5 wt% less MEA than the 30 wt% MEA solution. This means saving about 16% of MEA while

increasing the absorption rate. Given that MEA is a toxic and expensive chemical, having less MEA with a higher absorption rate benefits commercial and environmental aspects.

The other finding was CO_2 cyclic capacity, which was derived from the CO_2 loading plot. For all solutions and temperatures, there is no noticeable difference in the CO_2 cyclic capacity. It is concluded that adding glycerol to an aqueous MEA solution could maintain the CO_2 cyclic capacity over the temperature range of 313-333 K. However, the CO_2 cyclic capacity of this work's solution is lower than the other solutions in the literature. This is not desirable, as the low cyclic capacity leads to higher heat requirements for stripping, pump, and the heat exchanger's size and cost. Overall, it is concluded that the addition of 10 wt% glycerol to the aqueous MEA solution improved the absorption rate and CO_2 loading, but it has some drawbacks in terms of cyclic capacity. The results recommend adding 10 wt% glycerol to an aqueous MEA solution for the CO_2 absorption at atmospheric pressure, like post-combustion CO_2 capture. It is also recommended to extend the kinetic mechanism of the reaction between glycerol, MEA and CO_2 to develop a better understanding of the glycerol role.

Acknowledgement

The authors would like to acknowledge the Department of Chemical Engineering at the University of Malaya for supplying the facilities, chemicals and research material for this project.

Reference

[1] Z. Zhang, T.N.G. Borhani, M.H. El-Naas, Chapter 4.5 - Carbon Capture A2 - Dincer, Ibrahim, in: C.O. Colpan, O. Kizilkan (Eds.), Exergetic, Energetic and Environmental Dimensions, Academic Press2018, pp. 997-1016. https://doi.org/10.1016/B978-0-12-813734-5.00056-1.

[2] N.T. Borhani, M. Wang, Role of solvents in CO_2 capture processes: The review of selection and design methods, Renewable and Sustainable Energy Reviews 114 (2019) 109299. https://doi.org/10.1016/j.rser.2019.109299.

[3] Z. Zhang, T.N. Borhani, A.G. Olabi, Status and perspective of CO_2 absorption process, Energy 205 (2020) 118057. https://doi.org/10.1016/j.energy.2020.118057.

[4] T.N. Borhani, A. Azarpour, V. Akbari, S.R. Wan Alwi, Z.A. Manan, CO_2 capture with potassium carbonate solutions: A state-of-the-art review, International Journal of Greenhouse Gas Control 41 (2015) 142-162. https://doi.org/10.1016/j.ijggc.2015.06.026.

[5] T.N. Borhani, M. Afkhamipour, A. Azarpour, V. Akbari, S.H. Emadi, Z.A. Manan, Modeling study on CO_2 and H_2S simultaneous removal using MDEA solution, Journal of Industrial and Engineering Chemistry 34 (2016) 344-355. https://doi.org/10.1016/j.jiec.2015.12.003.

[6] S. Moioli, L.A. Pellegrini, M.T. Ho, D.E. Wiley, A comparison between amino acid based solvent and traditional amine solvent processes for CO_2 removal, Chemical Engineering Research and Design 146 (2019) 509-517. https://doi.org/10.1016/j.cherd.2019.04.035.

[7] S. Babamohammadi, A. Shamiri, M.K. Aroua, A review of CO_2 capture by absorption in ionic liquid-based solvents, Reviews in Chemical Engineering 31(4) (2015) 383. https://doi.org/10.1515/revce-2014-0032.

[8] Y. Zhang, X. Ji, X. Lu, Choline-based Deep Eutectic Solvents for CO_2 separation: Review and thermodynamic analysis, Renewable and Sustainable Energy Reviews 97 (2018) 436-455. https://doi.org/10.1016/j.rser.2018.08.007.

[9] G. Siani, M. Tiecco, P. Di Profio, S. Guernelli, A. Fontana, M. Ciulla, V. Canale, Physical absorption of CO_2 in betaine/carboxylic acid-based Natural Deep Eutectic Solvents, Journal of Molecular Liquids 315 (2020) 113708. https://doi.org/10.1016/j.molliq.2020.113708.

[10] M.S. Alivand, O. Mazaheri, Y. Wu, G.W. Stevens, C.A. Scholes, K.A. Mumford, Development of aqueous-based phase change amino acid solvents for energy-efficient CO_2 capture: The role of antisolvent, Applied Energy 256 (2019) 113911. https://doi.org/10.1016/j.apenergy.2019.113911.

[11] M.S. Alivand, O. Mazaheri, Y. Wu, G.W. Stevens, C.A. Scholes, K.A. Mumford, Preparation of Nanoporous Carbonaceous Promoters for Enhanced CO_2 Absorption in Tertiary Amines, Engineering 6(12) (2020) 1381-1394. https://doi.org/10.1016/j.eng.2020.05.004.

[12] A. Shamiri, M.S. Shafeeyan, H.C. Tee, C.Y. Leo, M.K. Aroua, N. Aghamohammadi, Absorption of CO_2 into aqueous mixtures of glycerol and monoethanolamine, Journal of Natural Gas Science and Engineering 35, Part A (2016) 605-613. https://doi.org/10.1016/j.jngse.2016.08.072.

[13] S. Mirzaei, A. Shamiri, M.K. Aroua, CO_2 absorption/desorption in aqueous single and novel hybrid solvents of glycerol and monoethanolamine in a pilot-scale packed bed column, Energy & Fuels 34(7) (2020) 8503-8515. https://doi.org/10.1021/acs.energyfuels.8b04389.

[14] S.A.N.M. Rahim, C.S. Lee, F. Abnisa, M.K. Aroua, W.A.W. Daud, P. Cognet, Y. Pérès, A review of recent developments on kinetics parameters for glycerol electrochemical conversion – A by-product of biodiesel, Science of The Total Environment 705 (2020) 135-137. https://doi.org/10.1016/j.scitotenv.2019.135137.

[15] H.W. Tan, A.R. Abdul Aziz, M.K. Aroua, Glycerol production and its applications as a raw material: A review, Renewable and Sustainable Energy Reviews 27 (2013) 118-127. https://doi.org/10.1016/j.rser.2013.06.035.

[16] P. Mario, R. Michele, Chapter 1 Glycerol: Properties and Production, The Future of Glycerol (2), The Royal Society of Chemistry (2010), pp. 1-28. https://doi.org/10.1039/9781849731089-00001.

[17] T.L. Ooi, K.C. Yong, K. Dzulkefly, W.M.Z. Wan Yunus, A.H. Hazimah, Crude Glycerine Recovery From Glycerol Residue Waste From A Palm Kernel Oil Methyl Ester Plant, Journal Of Oil Palm Research 13(2) (2001) 16-22.

[18] J.G. Speight, Chemical Process and Design Handbook, First edition. ed., McGraw-Hill Education, New York, 2002.

[19] S.J. López, M.M.L. Santos, C.A. Pérez, M.A. Martín, Anaerobic digestion of glycerol derived from biodiesel manufacturing., Bioresource Technology 100(23) (2009) 5609-5615. https://doi.org/10.1016/j.biortech.2009.06.017.

[20] P. Valeh-e-Sheyda, J. Barati, Mass transfer performance of carbon dioxide absorption in a packed column using monoethanoleamine-Glycerol as a hybrid solvent, Process Safety and Environmental Protection 146 (2021) 54-68. https://doi.org/10.1016/j.psep.2020.08.024.

[21] S. Babamohammadi, A. Shamiri, T.N. Borhani, M.S. Shafeeyan, M.K. Aroua, R. Yusoff, Solubility of CO_2 in aqueous solutions of glycerol and monoethanolamine, Journal of Molecular Liquids 249 (2018) 40-52. https://doi.org/10.1016/j.molliq.2017.10.151.

[22] H. Rashidi, S. Mamivand, Experimental and numerical mass transfer study of carbon dioxide absorption using Al2O3/water nanofluid in wetted wall column, Energy 238 (2022) 121670. https://doi.org/10.1016/j.energy.2021.121670.

[23] P. Valeh-e-Sheyda, A. Afshari, A detailed screening on the mass transfer modeling of the CO2 absorption utilizing silica nanofluid in a wetted wall column, Process Safety and Environmental Protection 127 (2019) 125-132. https://doi.org/10.1016/j.psep.2019.05.009.

[24] J. Kim, H. Kim, J. Kim, S.J. Hwang, K.S. Lee, Experimental method for simultaneous and continuous measurement of absorption rate, viscosity and heat of reaction of carbon dioxide capture solvents, Journal of Industrial and Engineering Chemistry 61 (2018) 152-160. https://doi.org/10.1016/j.jiec.2017.12.012.

[25] L. Wang, S. An, S. Yu, S. Zhang, Y. Zhang, M. Li, Q. Li, Mass transfer characteristics of CO2 absorption into a phase-change solvent in a wetted-wall column, International Journal of Greenhouse Gas Control 64 (2017) 276-283. https://doi.org/10.1016/j.ijggc.2017.08.001.

[26] D. Song, G.T. Rochelle, Reaction kinetics of carbon dioxide and hydroxide in aqueous glycerol, Chemical Engineering Science 161 (2016) 151-158. https://doi.org/10.1016/j.ces.2016.11.048.

[27] A. Tunnat, P. Behr, K. Görner, Desorption Kinetics of CO2 from Water and Aqueous Amine Solutions, Energy Procedia 51 (2014) 197-206. https://doi.org/10.1016/j.egypro.2014.07.023.

[28] G. Puxty, R. Rowland, M. Attalla, Comparison of the rate of CO_2 absorption into aqueous ammonia and monoethanolamine, Chemical Engineering Science 65(2) (2010) 915-922. https://doi.org/10.1016/j.ces.2009.09.042.

[29] R. Dugas, G. Rochelle, Absorption and desorption rates of carbon dioxide with monoethanolamine and piperazine, Energy Procedia 1(1) (2009) 1163-1169. https://doi.org/10.1016/j.egypro.2009.01.153.

[30] Y. Yuan, G.T. Rochelle, CO_2 absorption rate in semi-aqueous monoethanolamine, Chemical Engineering Science 182 (2018) 56-66. https://doi.org/10.1016/j.ces.2018.02.026.

[31] L. Li, H. Li, O. Namjoshi, Y. Du, G.T. Rochelle, Absorption rates and CO_2 solubility in new piperazine blends, Energy Procedia 37 (2013) 370-385. https://doi.org/10.1016/j.egypro.2013.05.122.

[32] A. Ahmady, M.A. Hashim, M.K. Aroua, Absorption of carbon dioxide in the aqueous mixtures of methyldiethanolamine with three types of imidazolium-based ionic liquids, Fluid Phase Equilibria 309(1) (2011) 76-82. https://doi.org/10.1016/j.fluid.2011.06.029.

[33] M.M. Mshewa, Carbon Dioxide Desorption/absorption with Aqueous Mixtures of Methyldiethanolamine and Diethanolamine at 40 to 120°C, Rochelle Group, University of Texas at Austin, USA, 1995.

[34] M. Pacheco, Mass Transfer, Kinetics and Rate-Based Modeling of Reactive Absorption, Rochelle Group, The University of Texas, USA, 1998.

[35] P. Luis, Chapter 5 - Membrane contactors, in: P. Luis (Ed.), Fundamental Modelling of Membrane Systems, Elsevier(2018), pp. 153-208. https://doi.org/10.1016/B978-0-12-813483-2.00005-8.

[36] R.L. Pigford, Counter-Diffusion in a Wetted Wall Column, The University of Illinois, Urbana, Illinois, 1941.

[37] L. Li, Carbon Dioxide Solubility and Mass Transfer in Aqueous Amines for Carbon Capture., Faculty of Graduate School, University of Texas at Austin, USA, 2015.

[38] R.B. Bird, W.E. Stewart, E. Lightfoot, Transport Phenomena., 2nd ed., John Wiley & Sons(2002).

[39] C.H. Byers, C.J. King, Gas-liquid mass transfer with a tangentially moving interface: Part I. Theory, 13(4) (1967) 628-636. https://doi.org/10.1002/aic.690130409.

[40] L. Valenz, F.J. Rejl, J. Šíma, V. Linek, Absorption Mass-Transfer Characteristics of Mellapak Packings Series, Industrial & Engineering Chemistry Research 50(21) (2011) 12134-12142. https://doi.org/10.1021/ie200577k.

[41] H. Karlsson, H. Svensson, Rate of Absorption for CO_2 Absorption Systems Using a Wetted Wall Column, Energy Procedia 114 (2017) 2009-2023. https://doi.org/10.1016/j.egypro.2017.03.1335.

[42] K. Han, C.K. Ahn, J.Y. Kim, Absorbent characterization for CO_2 capture using wetted-wall column and reaction calorimetry, Energy Procedia 4 (2011) 548-553. https://doi.org/10.1016/j.egypro.2011.01.087.

[43] Y. Yuan, B. Sherman, G.T. Rochelle, Effects of viscosity on CO_2 absorption in aqueous piperazine/2-methylpiperazine, Energy Procedia 114 (2017) 2103-2120. https://doi.org/10.1016/j.egypro.2017.03.1345.

[44] D. Song, Effect of Liquid Viscosity on Liquid Film Mass Transfer for Packings, Faculty of Graduate School, University of Texas at Austin, USA, 2017.

[45] Y. Yuan, Mass Transfer Rate in Semi-Aqueous Amines for CO_2 Capture., Faculty of Graduate School, University of Texas at Austin, USA, 2018.

[46] F. Xu, H. Gao, H. Dong, Z. Wang, X. Zhang, B. Ren, S. Zhang, Solubility of CO_2 in aqueous mixtures of monoethanolamine and dicyanamide-based ionic liquids, Fluid Phase Equilibria 365 (2014) 80-87. https://doi.org/10.1016/j.fluid.2013.12.020.

[47] A. Schäffer, K. Brechtel, G. Scheffknecht, Comparative study on differently concentrated aqueous solutions of MEA and TETA for CO_2 capture from flue gases, Fuel 101 (2012) 148-153. https://doi.org/10.1016/j.fuel.2011.06.037.

[48] Z. Feng, F. Cheng-Gang, W. You-Ting, W. Yuan-Tao, L. Ai-Min, Z. Zhi-Bing, Absorption of CO_2 in the aqueous solutions of functionalized ionic liquids and MDEA, Chemical Engineering Journal 160(2) (2010) 691-697. https://doi.org/10.1016/j.cej.2010.04.013.